CrystEngComm

PAPER

View Article Online
View Journal | View Issue

Cite this: *CrystEngComm*, 2016, **18**, 7104

Investigation of structure-directing interactions within copper(I) thiocyanate complexes through X-ray analyses and non-covalent interaction (NCI) theoretical approach†

Khodayar Gholivand,*[a] Kaveh Farshadfar,[a] S. Mark Roe,[b] Mahdieh Hosseini[a] and Akram Gholami[a]

Received 10th June 2016,
Accepted 9th August 2016

DOI: 10.1039/c6ce01339b

www.rsc.org/crystengcomm

Herein, we reported the synthesis of copper(I) thiocyanate complexes with *ortho*-pyridinyl carbohydrazones containing a thiophene (L_1) or a furyl ring (L_2) as a mixture of two different crystals for each compound, linkage isomers of C_{1N}, [Cu(NCS)(L_1)PPh_3] and C_{1S}, [Cu(SCN)(L_1)PPh_3], for L_1, whereas monomeric and polymeric structures C_{2N}, [Cu(NCS)(L_2)PPh_3], and C_{2P}, [–(NCS)Cu(L_2)–]$_n$, for L_2. Crystallographic information and theoretical calculations, mainly noncovalent interaction reduced density gradient (NCI-RDG) analyses, were pursued to generate a profound understanding of the structure-directing interactions in these complexes. The supramolecular assemblies are first driven by cooperative π···π interactions and hydrogen bonds followed by CH···π, S···S and S···π linkages. In the case of the linkage isomers, intermolecular interactions may have a significant role in the formation of the less stable S-bound isomer C_{1S}.

Introduction

Copper(I) compounds have attracted a growing interest because of their high structural diversity,[1–4] catalytic activity[5–7] and photophysical properties.[3,8–10] They have applications in different areas such as organic light-emitting diodes (OLEDs),[11–22] supramolecular assemblies, oxygen sensors and biological probes. The rich structural features and utilitarian considerations have motivated researchers to focus on the synthesis and characterization of Cu(I) complexes with various donor ligands. The formation of structural variations is greatly influenced by several parameters such as the synthetic conditions or steric/electronic effects exerted by the ligand.

The triatomic pseudohalide, thiocyanate anion (SCN^-), is an excellent versatile ambidentate ligand with two donor atoms, S or N.[23] It can coordinate to metal ions both in terminal and bridging coordination modes and potentially provide fascinating examples of linkage isomerism.[24–26] When SCN^- acts as a terminal ligand, it affords potential interaction sites to generate non-covalent intermolecular interactions and, accordingly, can direct the crystal packing. Controlling the self-assemblies in the solid state on the basis of molecular structures and through the use of weak interactions is a long-standing goal of supramolecular chemistry.[27]

Very recently in our previous work, cuprous halide complexes of *ortho*-, *meta*- and *para*-pyridinyl carbohydrazones were introduced.[28] The influence of ligand structure and halide variations on the molecular structures and supramolecular arrays of the complexes were studied both experimentally and theoretically. In the following, we employed cuprous pseudohalide, CuSCN, for the synthesis of complexes with two *ortho*-pyridinyl carbohydrazones. Copper(I) thiocyanate compounds are very interesting in solar cell applications as a p-type semiconductor.[29–31]

In this contribution, we report the structural characteristics of complexes from the reaction of CuSCN with PPh_3 and

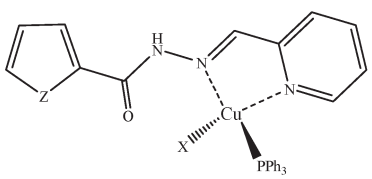

C_{1N}: Z = S, X = -NCS⁻
C_{1S}: Z = S, X = -SCN⁻
C_{2N}: Z = O, X = -NCS⁻
C_{2P}: Z = O, X = bridge -NCS⁻-, without PPh_3; polymer

Scheme 1

[a] *Department of Chemistry, Faculty of Science, Tarbiat Modares University, Tehran, Iran. E-mail: gholi_kh@modares.ac.ir*
[b] *Department of Chemistry, School of Life Sciences, University of Sussex, Brighton, BN1 9QJ, UK*

† Electronic supplementary information (ESI) available: IR and NMR spectra of all compounds and crystallographic files in CIF format for structural determination of complexes. CCDC 1401344, 1401345, 1469718 and 1469717. For ESI and crystallographic data in CIF or other electronic format see DOI: 10.1039/c6ce01339b

ortho-pyridinyl carbohydrazones containing a thiophene (L_1) or a furyl ring (L_2); see Scheme 1. The former resulted in two linkage isomers: C_{1N} [Cu(NCS)(L_1)PPh_3] and C_{1S} [Cu(SCN)(L_1)-PPh_3], while the later afforded monomeric and polymeric complexes of C_{2N} [Cu(NCS)(L_2)PPh_3] and C_{2P} [–(NCS)Cu(L_2)–]$_n$. We have also used a recently introduced alternative interpretive technique, the non-covalent interaction (NCI) approach, to manifest the diverse NCIs at the crystal packing structures. This method is based on the analysis of the electron density and enables us to identify and visualize the interactions.[32] Various non-covalent interactions, including hydrogen bonding,[33] S···S, S···π,[34] π···π[35] and CH···π[36] interactions, have been investigated in this work.

Results and discussion

Synthesis

Ligands L_1 and L_2 were prepared by mixing equivalent amounts of 2-thiophenecarboxylic acid hydrazide (1) or furoic hydrazide (2) and 2-pyridinecarboxaldehyde in methanol solution.

A solution of the ligand in $CHCl_3$ was added dropwise to a mixture of copper(I) thiocyanate and PPh_3 while stirring in CH_3CN and then the mixture was filtered off. After slow diffusion of diethyl ether in the filtered solutions, two different crystals were obtained for each compound including the light orange needle crystals (C_{1N}) and clear light red irregular crystals (C_{1S}) for L_1 and orange needle crystals (C_{2N}) and dark orange hexagonal crystals (C_{2P}) for L_2. A mixture of the isomeric crystals C_{1N} and C_{1S} is shown in Fig. 1.

Various ratios of acetonitrile and chloroform solvents were assessed in the crystallization of C_1. Upon using more chloroform, the percentage of C_{1N} was dominant, whereas a higher amount of acetonitrile in the reaction pot increased the percentage of C_{1S}. For C_2, the formation of crystals depended on the concentration of the reaction mixture. At a high concentration, the polymeric compound precipitated fast and we only obtained crystals of C_{2N}, but slower diffusion of diethyl ether in the more dilute solution afforded crystals of both C_{2P} (as the dominant product) and C_{2N} suitable for X-ray diffraction.

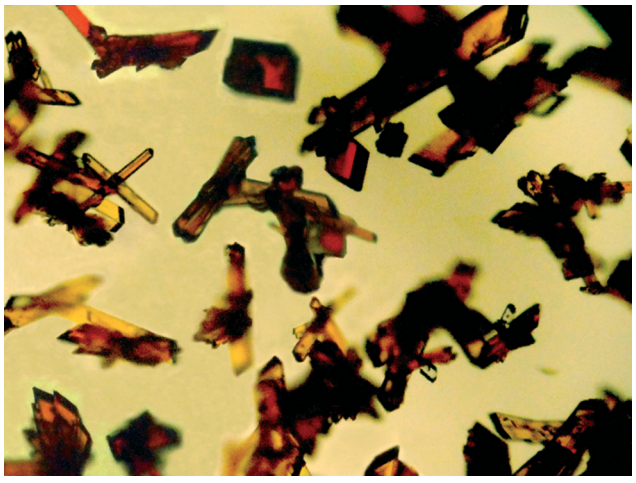

Fig. 1 50× magnification photo of a mixture of orange rectangular cube C_{1N} and red cube C_{1S}.

ORTEP diagrams of the molecular structures are shown in Fig. 2. The crystallographic data of the complexes are listed in Table 1. Selected bond distances and angles are summarized in Table 2.

Structural analysis

Cu(NCS)(L_1)PPh_3] (C_{1N}). The title compound crystallizes in the triclinic space group $P\bar{1}$. Ligand L_1 binds to the copper atom in a bidentate chelating manner *via* N2 (pyridine) and N3 (imine). An isothiocyanate anion (N-donor) and one PPh_3 occupy the other coordination sites (Fig. 1). Houser and coworkers suggested an angular index (τ_4) which determines the geometry of the four-coordinate metal centres as follows: $\tau_4 = [360 - (\alpha + \beta)]/141]$ (α and β are the two largest angles around a four-coordinate metal centre). The values of τ_4 will range from 1.00 for a perfect tetrahedral geometry to zero for a perfect square planar environment. Intermediate structures including trigonal pyramid and seesaws fall within the range of 0 to 1.00.[37] According to the τ_4 value for C_{1N} (0.79), the coordination polyhedra of the copper centre can be described as trigonal pyramid.

In the structure of C_{1N}, each molecular unit of the complex is joined to the neighbouring unit by means of three 2-fold interactions including classical and non-classical hydrogen bonds N4–H4···S1 and C7–H7···S1, respectively (Table 3), and π_{py}–$\pi_{thiophene}$ interactions (Table 4).

The dimers are further connected to each other through π_{py}–π_{py} and C5–H5···π_{PPh3} interactions along the *a*-direction (Fig. 3a) to afford chains which are laterally linked together *via* various intermolecular interactions to generate a 3D network. The interactions which link the chains along the *b*-axis include (i) S1···S1, (ii) C3H3···S1, (iii) C11–H11···π_{py}, (iv) C2–H2···$\pi_{thiophene}$ and (v) C14–H14···$\pi_{thiophene}$ linkages (Fig. 3b). In addition, C21H21···S2 H-bonds plus weak C27–H27···π_{PPh3} interactions (C···Cg: 4.090 Å) connect them along the *c*-direction (Fig. 3c). The distance of the S···S interaction was found to be about 3.456 Å which is 4% shorter than the sum of the van der Waals radii of two sulfur atoms. A summary of the parameters for the other interactions mentioned above are presented in Tables 3 and 4.

[Cu(SCN)(L_1)PPh_3] (C_{1S}). The red irregular crystals of C_{1S} are the second form resulting from the reaction of a 1 : 1 molar ratio of L_1 and the mixture of cuprous thiocyanate and PPh_3. X-ray diffraction analysis reveals that it crystallizes in the triclinic space group $P\bar{1}$. The central copper atoms are again in trigonal pyramidal environments (τ_4 = 0.82, exactly equal to that for C_{1N}) formed by N_{py} and N_{im} (from the chelating ligand), PPh_3 moiety and thiocyanate anion (this time as an S-donor) (Fig. 1). Changing the coordination site of the ambidentate ligand, NCS^-, alters the supramolecular architecture of C_{1S} compared to that of the N-bound isomer C_{1N}.

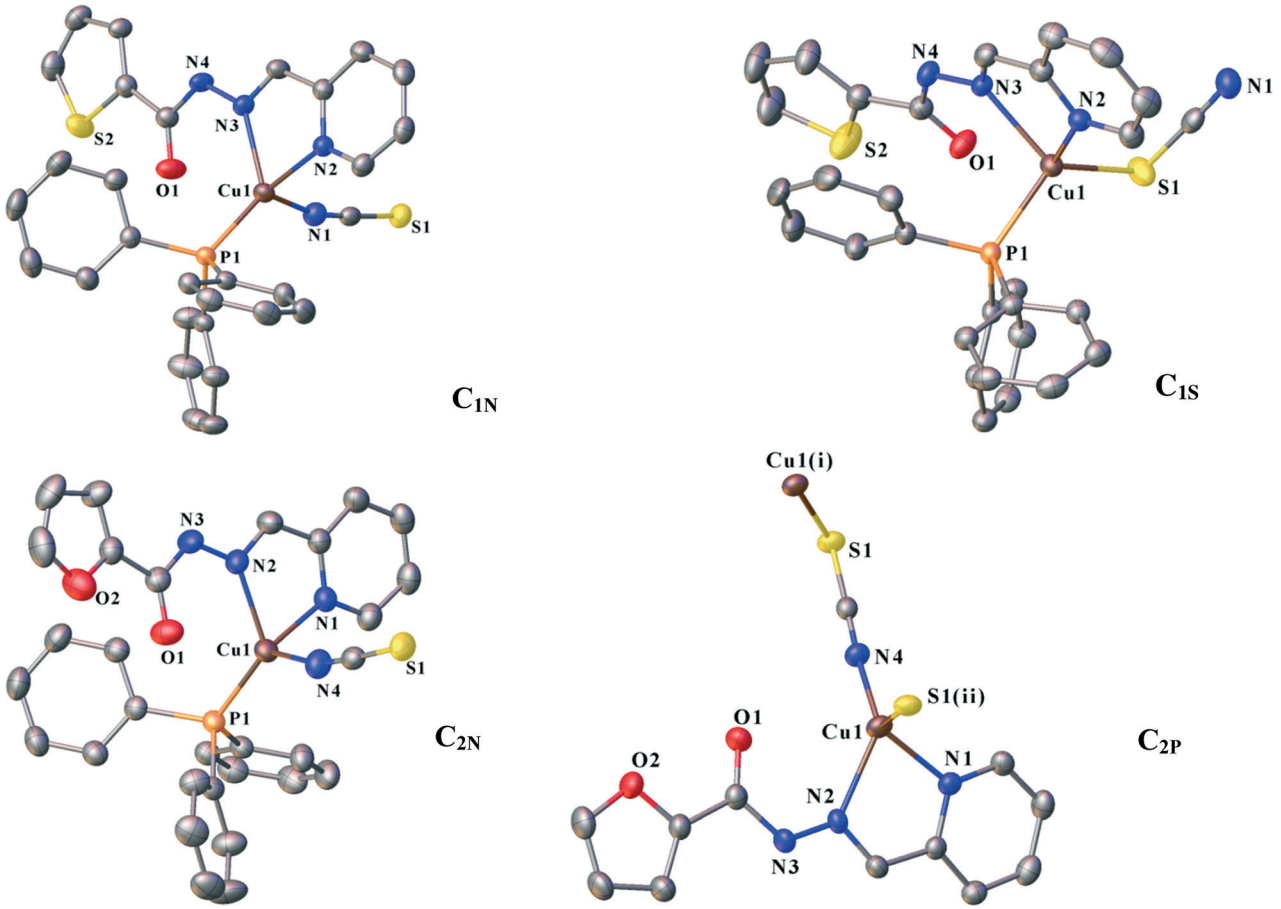

Fig. 2 ORTEP diagrams of C_{1N}, C_{1S}, C_{2N} and C_{2P} with displacement ellipsoid at the 50% level. Hydrogen atoms were omitted for clarity. Symmetry codes: (i) x, 1/2 − y, 1/2 + z; (ii) x, 1/2 − y, −1/2 + z.

Table 1 Crystal data and structural refinement parameters for compounds C_{1N}, C_{1S}, C_{2N} and C_{2P}

Compound	C_{1N}	C_{1S}	C_{2N}	C_{2P}
Formula	$C_{30}H_{24}CuN_4OPS_2$	$C_{30}H_{24}CuN_4OPS_2$	$C_{30}H_{24}CuN_4O_2PS$	$C_{12}H_9CuN_4O_2S$
Fw	615.16	615.16	599.10	336.83
λ/Å	1.54184	0.71073	1.54184	1.54184
T/K	173	173	173	173
Crystal system	Triclinic	Triclinic	Triclinic	Monoclinic
Space group	$P\bar{1}$	$P\bar{1}$	$P\bar{1}$	$P21/c$
a/Å	9.8334(5)	10.7768(9)	9.8386(7)	15.7005(7)
b/Å	10.2673(6)	11.0362(8)	10.1356(6)	8.0099(4)
c/Å	15.0986(9)	12.2584(5)	14.9963(10)	10.3633(5)
α/°	87.742(5)	85.195(5)	90.004(5)	90
β/°	89.510(4)	78.024(5)	90.051(6)	94.374(4)
γ/°	66.545(5)	80.116(6)	113.105(7)	90
V/Å^3	1397.31(15)	1403.30(17)	1375.48(17)	1299.49(11)
D_{calc}/Mg m^{-3}	1.462	1.456	1.447	1.722
Z	2	2	2	4
μ/mm^{-1}	3.292	1.015	2.666	3.948
F(000)	632	632	616	680
2θ/°	142.128	59	143	142
R(int)	0.025	0.030	0.030	0.041
GOOF	1.022	1.11	1.04	1.03
R_1 ($I > 2\sigma(I)$)	0.0295	0.0444	0.0373	0.0356
wR_2 ($I > 2\sigma(I)$)	0.0778	0.1072	0.1078	0.0955

The crystal structure of C_{1S} contains hydrogen bonded dimers generated by three pairwise interactions, N4–H4···N1, C7–H7···N1 and C10–H10···N1 (Table 3 and Fig. 4a). It is worth noting that the coordination of sulfur to the Cu(I) atom

Table 2 Selected bond lengths (Å) and angles (°) around copper(I) for complexes C_{1N}, C_{1S}, C_{2N} and C_{2P}

C_{1N}			
Cu1–P1	2.1880(6) Å	Cu1–N2	2.1367(16) Å
Cu1–N1	1.979(18) Å	Cu1–N3	2.1501(16) Å
P1–Cu1–N1	119.83(5)°	N1–Cu1–N2	99.81(7)
P1–Cu1–N2	121.68(5)°	N1–Cu1–N3	101.96(7)
P1–Cu1–N3	126.46(4)°	N2–Cu1–N3	77.56(6)
C_{1S}			
Cu1–S1	2.2936(9) Å	Cu1–N2	2.050(2) Å
Cu1–P1	2.1990(7) Å	Cu1–N3	2.181(2) Å
S1–Cu1–P1	117.60(3)°	P1–Cu1–N2	117.49(6)°
S1–Cu1–N2	107.38(6)°	P1–Cu1–N2	103.74(6)°
S1–Cu1–N3	127.28(6)°	N2–Cu1–N3	77.65(8)°
C_{2N}			
Cu1–P1	2.1893(6) Å	Cu1–N2	2.1547(19) Å
Cu1–N1	2.1411(19) Å	Cu1–N4	1.983(2) Å
P1–Cu1–N1	121.44(6)°	N1–Cu1–N2	77.23(7)°
P1–Cu1–N2	126.25(5)°	N1–Cu1–N4	98.52(8)°
P1–Cu1–N4	121.53(7)°	N2–Cu1–N4	101.32(8)°
C_{2P}			
Cu1–N1	2.105(2) Å	Cu1–N4	1.906(2) Å
Cu1–N2	2.131(2) Å	Cu1–S1	2.2971(8) Å
N1–Cu1–N2	77.74(9)°	N2–Cu1–N4	130.03(9)°
N1–Cu1–N4	109.43(9)°	N2–Cu1–S1	103.43(7)°
N1–Cu1–S1	111.59(7)°	N4–Cu1–S1	117.54(7)°

and consequently the orientation of the N1 atom direct the formation of hydrogen bonds and lead to supernumerary slippage of molecules on each other. The offset of pyridine and thiophene rings prevents the formation of a π_{py}–$\pi_{thiophene}$ interaction, unlike in the structure C_{1N}. Thus, instead of a π_{py}–$\pi_{thiophene}$ interaction, a C=O···π interaction is established between the discrete molecules in the dimers. In addition, S···S interactions connect the dimers to form [001] chains. The distance between two sulfur atoms is equal to 3.594 Å. These chains are held together by C11–C11···π_{PPh3} and C17–H17···$\pi_{thiophene}$ linkages (Table 4) along the *a*- and *b*-directions, respectively, which complete a 3D network (Fig. 4b–d).

$[Cu(NCS)(L_2)PPh_3]$ (C_{2N}). This compound crystallizes in the triclinic space group $P\bar{1}$. A trigonal pyramidal configuration of the Cu(I) centres (τ_4 = 0.80) has been formed by the bidentate chelating ligand, PPh_3 and isothiocyanate (N-donor). C_{2N} has a similar coordination environment to that of C_{1N} leading to its being isostructural with this complex. The supramolecular organization of C_{2N} is also disciplined by the formation of dimers through the same kind of interactions in C_{1N}: N3–H3···S1, C6–H6···S1 and π_{py}–π_{furyl} stacking interactions. Pyridine rings participate in the other π–π interactions (π_{py}–π_{py}) which build up a chain of the dimers directed along the *c*-axis. The chains are further reinforced by C3–H3A···π_{PPh3} and C4–H4···π_{PPh3} contacts (see Table 4). On the other hand, S···S synthons accompanied by C2–H2···S1, C15–H15···S1 and C10–H10···N4 hydrogen bonds as well as C1–H1···π_{furyl} interactions link the chains to create (110) sheets. The third dimension of the supramolecular assembly results from the connection of the layers *via* C21–H21···π_{furyl} linkages. Crystal packing diagrams of C_{2N} are presented in Fig. 5.

$[-(NCS)Cu(L_2)-]_n$ (C_{2P}). The reaction of a 1 : 1 molar ratio of L_2 with the mixture of CuSCN and PPh_3 results in two kinds of crystals: orange needle crystals, C_{2N}, and dark orange hexagonal ones, C_{2P}. X-ray diffraction analysis confirms that C_{2P} crystallizes in the monoclinic space group $P2_1/c$. Unlike the former complexes, PPh_3 does not coordinate to copper(I). In return, the trigonal pyramid geometry of the Cu(I) centre (τ_4 = 0.80) consists of the chelating ligand (L_2), thiocyanate (–SCN) and isothiocyanate (–NCS). Indeed, each thiocyanate anion acts as a bridge between the Cu(I) ions through simultaneous binding from S and N atoms. This coordination pattern leads to the formation of infinite polymeric chains extended along the *c*-axis (Fig. 6a). The Cu···Cu distance within the metal chain is 5.323 Å. The chains are further stabilized *via* intrachain hydrogen bonds (N3–H3···O1, C9–H9···O2 and C4–H4···S1).

Although the coordination structure of C_{2P} is different from the others, π–π interactions still have an important

Table 3 Hydrogen bond geometries for compounds C_{1N}, C_{1S}, C_{2N} and C_{2P}

Structure	D–H···A	*d* D–H	*d* H···A	*d* D···A	∠ D–H···A	Symm. codes
C_{1N}	N4–H4···S1	0.880	2.6800	3.5042(18)	157.00	1 − *x*, 1 − *y*, 1 − *z*
	C7–H7···S1	0.950	2.8700	3.6680(2)	143.00	1 − *x*, 1 − *y*, 1 − *z*
	C3–H3···S1	0.930	2.8754	3.7910(2)	162.00	−*x*, 2 − *y*, 1 − *z*
	C21–H21···S2	0.930	3.0230	3.5480(2)	116.00	1 − *x*, 1 − *y*, 2 − *z*
C_{1S}	C10–H10···N1	0.950	2.5580	3.4540(4)	157.30	1 − *x*, 1 − *y*, 1 − *z*
	C7–H7···N1	0.950	2.7990	3.5690(5)	138.80	1 − *x*, 1 − *y*, 1 − *z*
	N4–H4···N1	0.880	2.2330	3.0760(3)	163.16	1 − *x*, 1 − *y*, 1 − *z*
C_{2N}	N3–H3···S1	0.879	2.6810	3.4930(2)	153.90	1 − *x*, 1 − *y*, 1 − *z*
	C6–H6···S1	0.949	2.8469	3.6410(3)	141.80	1 − *x*, 1 − *y*, 1 − *z*
	C10–H10···N4	0.950	2.7230	3.5320(3)	143.60	1 + *x*, 1 + *y*, *z*
	C2–H2···S1	0.950	2.8812	3.8020(2)	163.60	2 − *x*, 2 − *y*, 1 − *z*
	C15–H15···S1	0.950	2.9839	3.8270(3)	148.60	*x*, −1 + *y*, *z*
C_{2P}	C9–H9···O2	0.950	2.4970	3.3940(4)	157.40	*x*, 1/2 − y, −1/2 + *z*
	N3–H3···O1	0.880	2.3140	3.1000(3)	148.70	*x*, 1/2 − *y*, −1/2 + *z*
	C2–H2···N4	0.950	2.6850	3.5830(4)	157.90	2 − *x*, 1/2 + *y*, 1/2 − *z*
	C11–H11···N4	0.950	2.5310	3.3480(4)	144.10	1 − *x*, −1/2 + *y*, 1/2 − *z*
	C11–H11···O1	0.950	2.6870	3.1830(4)	113.10	1 − *x*, −1/2 + *y*,1/2 − *z*

Table 4 π. interaction geometries for compounds C_{1N}, C_{1S}, C_{2N} and C_{2P}

Structure	Interaction	C–C (Å)	P–P°	P–CC°	CH···CgI	C···Cg (Å)	C–H–Cg (°)	Symm. code
C_{1N}	π_{py}–$\pi_{thiophene}$	3.749	7.52	19.63 27.14	—	—	—	1 − *x*, 1 − *y*, 1 − *z*
	π_{py}–π_{py}	3.486	0.0	7.88	—	—	—	−*x*, 1 − *y*, 1 − *z*
	CH···π_{PPh3}	—	—	—	C4–H4A···Cg6	3.725	165.63	−*x*, 1 − *y*, 1 − *z*
	CH···π_{PPh3}	—	—	—	C5–H5···Cg4	2.689	145.87	−*x*, 1 − *y*, 1 − *z*
	CH···π_{py}	—	—	—	C11–H11···Cg3	3.737	134.12	1 + *x*, −1 + *y*, *z*
	CH···$\pi_{thiophene}$	—	—	—	C14–H14···Cg2	3.134	145.84	−1 + *x*, 1 + *y*, *z*
	CH···$\pi_{thiophene}$	—	—	—	C2–H2···Cg2	3.592	134.97	−1 + *x*, 1 + *y*, *z*
C_{1S}	Amide···π_{py}	3.403	—	—	—	—	—	1 − *x*, 1 − *y*, 1 − *z*
	CH···π_{PPh3}	—	—	—	C11–H11···Cg7	2.749	141.19	1 + *x*, *y*, *z*
	CH···π_{PPh3}	—	—	—	C17–H17···Cg7	3.275	132.77	1 − *x*, −*y*, 2 − *z*
C_{2N}	π_{py}–π_{furyl}	3.719	11.74	17.28 28.73	—	—	—	1 − *x*, 1 − *y*, 1 − *z*
	π_{py}–π_{py}	3.461	0.0	5.15	—	—	—	2 − *x*, 1 − *y*, 1 − *z*
	CH···π_{furyl}	—	—	—	C1–H1···Cg2	3.602	135.83	1 + *x*, 1 + *y*, *z*
	CH···π_{PPh3}	—	—	—	C4–H4···Cg6	2.721	145.84	2 − *x*, 1 − *y*, 1 − *z*
	CH···π_{PPh3}	—	—	—	C3–H3A···Cg4	3.761	166.03	2 − *x*, 1 − *y*, *z*
C_{2P}	S···π_{py}	3.882	—	19.60	—	—	—	*x*, *y*, 1 + *z*
	π_{py}–π_{py}	3.801	0.0	28.19	—	—	—	2 − *x*, 1 − *y*, −*z*
	π_{furyl}–π_{furyl}	3.583	0.0	17.13	—	—	—	1 − *x*, −*y*, −*z*

Cg stands for the centre of gravity of the mentioned ring: for C_{1N}: **Cg2**: S2, C9–C12; **Cg3**: N2, C2–C6; **Cg4**: C13–C18; **Cg6**: C25–C30; for C_{1S}: **Cg7**: C25–C30; for C_{2N}: **Cg2**: O2, C8–C11; **Cg4**: C13–C18; **Cg6**: C25–C30; for C_{2P}: **Cg2**: O2, C8–C11; **Cg3**: N1, C1–C5.

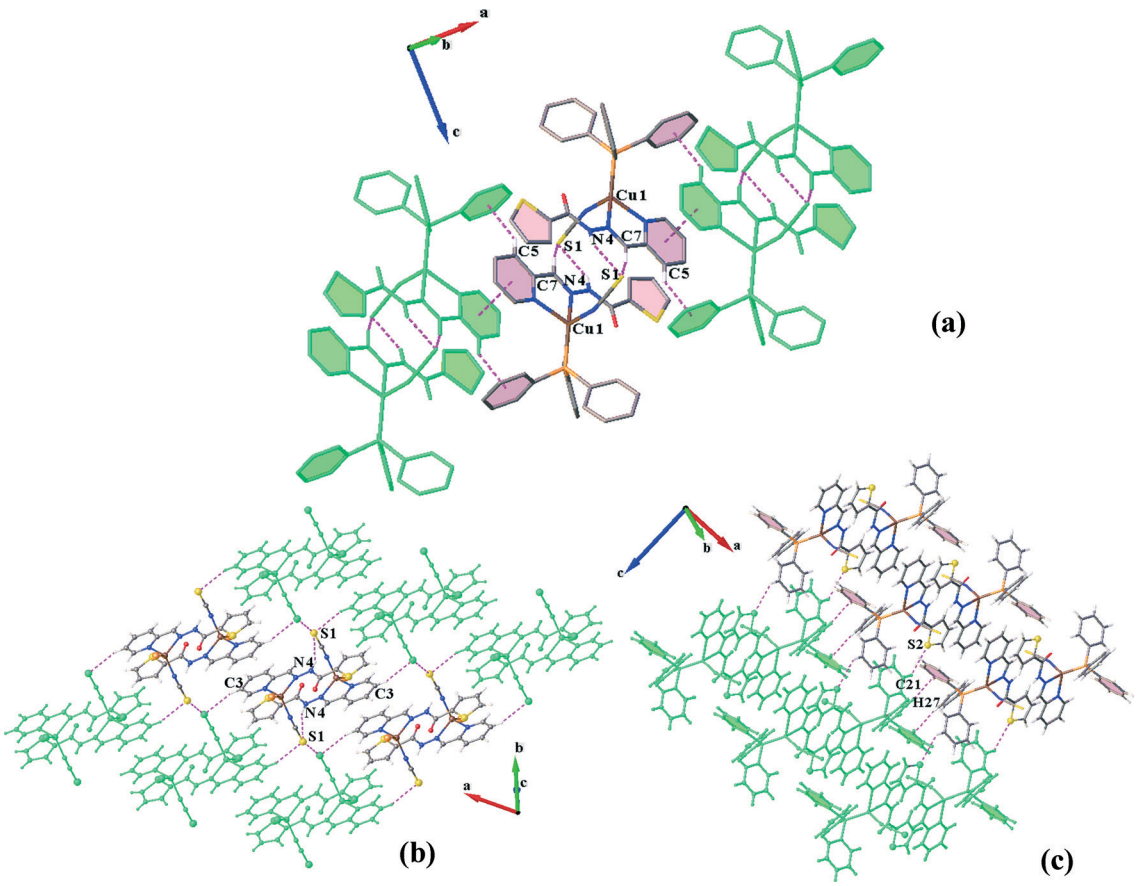

Fig. 3 (a) Representation of dimeric units in C_{1N} and their association through π–π and C–H···π interactions, creating the [100] chain; (b and c) side views of the crystal packing in the *ac* and *ab* planes, respectively, which show how the chains are connected in the 3D network.

contribution in the crystal packing. Herein, π_{furyl}–π_{furyl} interactions establish two-fold sheets of the neighbouring chains which are also fortified by bifurcated hydrogen bonds. The other side of the chains in the sheets is involved in π_{py}–π_{py}

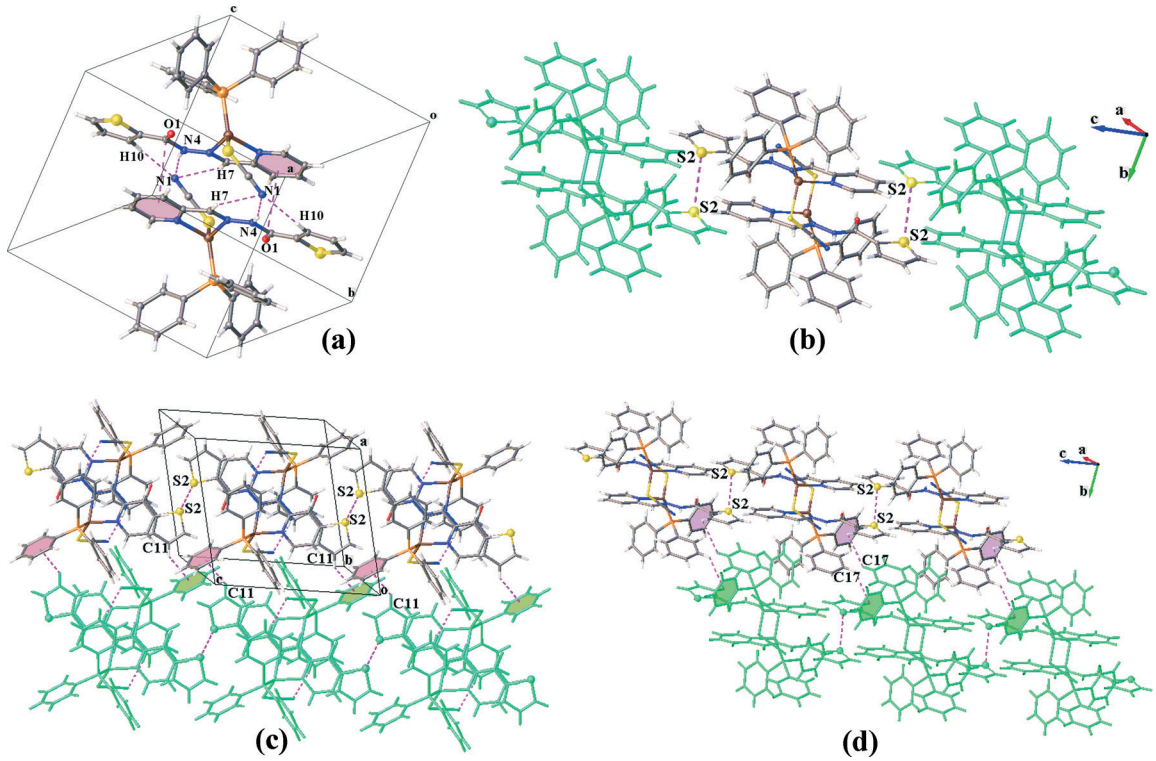

Fig. 4 Self-assembly of C_{1S}: (a) dimeric aggregates formed by pairwise H-bonds and C=O···π linkages; (b) S···S interactions generating [001] chains; (c and d) C–H···π interactions which link the chains in the *ac* and *ab* planes, respectively.

stacking and H-bonding interactions, leading to the connection of the (011) layers along the *a*-direction to complete the overall supramolecular association (Fig. 6b). In other words, each coordination chain is associated with four other chains in a 3D arrangement, from one side through π_{furyl}–π_{furyl}, C11–H11···N4 and C11–H11···O1 linkages and from the other side by π_{py}–π_{py} stacking and C2–H2···N4 interactions (Fig. 6c). In addition, these chains are laterally linked through interesting S···π_{py} interactions in the *b*-direction (Fig. 6d).

NCI approach

Principle. The non-covalent interaction (NCI) reduced density gradient (RDG) method has been recently developed as a theoretical strategy to visualize weak interactions. Investigation of the interactions using NCI-RDG analysis is quite concordant with the traditional method that recognizes them according to distances and angles. However, the NCI-RDG technique has more accuracy and precision, as it is based on fundamental computation. It provides a rich illustration of strong attractive, van der Waals interactions and also steric repulsions. The theory rests on the analysis and the graphical interpretation of two scalar properties, charge density ρ and its derivatives, namely the λ eigenvalue of its Hessian and its reduced gradient $s(\rho)$,[22] defined as:

$$s = \frac{1}{2(3\pi^2)^{1/3}} \frac{|\nabla\rho|}{\rho^{4/3}}$$

where $\nabla\rho$ is the gradient of ρ. The non-covalent interactions are located in the regions with low RDG and density. Analysis of sign(λ_2) of the electron density Hessian can be used to discern different types of interactions. For the strong ones such as H-bonds, sign(λ_2)$\rho < 0$; for the weak van der Waals types, sign(λ_2)$\rho \approx 0$; and for the non-bonded interactions like steric repulsion, sign(λ_2)$\rho > 0$.

As the sign of λ_2 describes the essence of the interaction, 2D plots comprising sign(λ_2) × ρ *versus* RDG *s* would indicate a non-covalent interaction near-zero area in the horizontal axis.[38–44] Close contacts between atoms change the behaviour of the reduced gradient signal more compared to the contacts among the atoms present in the tails, leading to troughs in the 2D NCI plots. These troughs, specially the ρ value at the troughs, are the basis of the NCI approach. The 2D NCI plots are then applied as inputs to construct 3D NCI plots, including isosurfaces of the reduced gradient of the density enabling the spatial visualization of the close contacts.

We applied this method to unravel the nature of supramolecular interactions in the title complexes. NCI analysis has been performed on the structure of complexes including the diverse noncovalent interactions. The considered structures were cut out directly from the CIF data. Since dimerization is the prominent feature of the crystal packing in the monomeric complexes (C_{1N}, C_{1S} and C_{2N}), the main NCIs are related to the interactions involved in the formation of dimers. The 2D and 3D NCI plots of dimers are shown in Fig. 7. Accordingly, we have done calculation once on the dimers

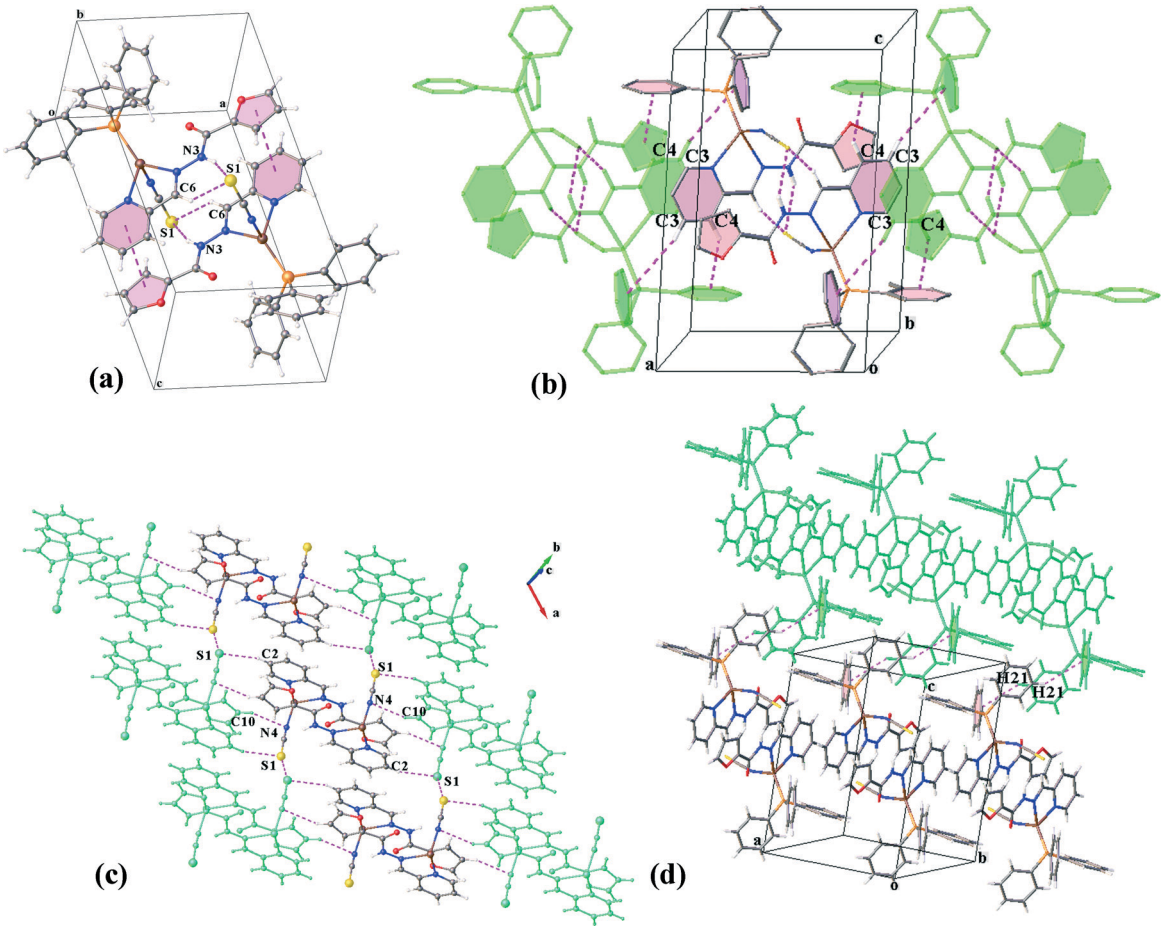

Fig. 5 (a) Representation of dimeric units in C_{2N}; (b) association of these units through π–π and C–H···π interactions, creating the [100] chain; (c and d) side views of the crystal packing in the *ab* and *ac* planes, respectively; which show how the chains are connected in the 3D construction (PPh_3 moieties in (c) were omitted for more clarity).

including only the carbohydrazone ligands (Cu^+ and SCN^- ions and PPh_3 moieties have been eliminated) and again for the whole dimeric units of complexes. Some of the other interesting intermolecular interactions in the crystal structures have also been investigated by the NCI method. The presence of noncovalent interactions is characterized by spikes at negative to near-zero sign of λ_2, whereas the peaks at positive sign indicate the repulsive steric contacts due to the ring formation.[45] The spikes at the zero area ($\text{sign}(\lambda_2)\rho$ between ±0.015 a.u.) show vdW interactions. Notable points of the NCI calculations have been illustrated in the following:

(i) As shown in Fig. 7, for the ligand dimers, the spikes that appeared at 0.024 a.u. belong to the pyridine ring closure. These spikes shift to lower values (less repulsion) in the whole dimeric units of complexes. It can be explained by the effect of metal ion in the charge redistribution as well as the electrostatic interaction between atoms within the rings.

(ii) In the case of C_{1N}, the thiophene ring closure spike ($\text{sign}(\lambda_2)\rho$) is located between 0.042 and 0.044 a.u. while in the 2D plot and the 3D isosurface of C_{2N}, the furyl ring has a much lesser repulsion of ring closure than the thiophene alternative. It may be caused by the greater charge perturbation due to the presence of an oxygen atom which leads to more electrostatic interactions. Consistent with this, natural bond orbital (NBO) analysis also reveals the stabilizing energy of 54 kcal mol^{-1} for the electronic delocalization "lone pair (O) → π* (C–C) orbital" which is more than that for the corresponding charge transfer energy in the thiophene ring (LP(S) → π*(C–C): 48 kcal mol^{-1}).

(iii) C_{1N} and C_{1S} compounds are linkage isomers, in a way that SCN^- is coordinated from N or S atoms, respectively. Optimization of the isomers, in the gas phase and also acetonitrile and chloroform solutions, indicates that the stability of C_{1S} is approximately 3–4 kcal mol^{-1} less than that of C_{1S}; however, it has been also formed in the solid state. The formation of C_{1S} can be attributed to stronger intermolecular attractions particularly those involved in dimerization which compensate for the lesser stability of the discrete units of C_{1S}. RDG isosurfaces show stronger interactions in the C_{1S} dimer rather than in C_{1N}. Counterpoise calculations at the M06-2X/6-311G* level indicate that the binding energy of two complexes in a dimer, ΔE_{dimer}, for C_{1S} is 2.8 kcal mol^{-1} more than for C_{1N} as well.

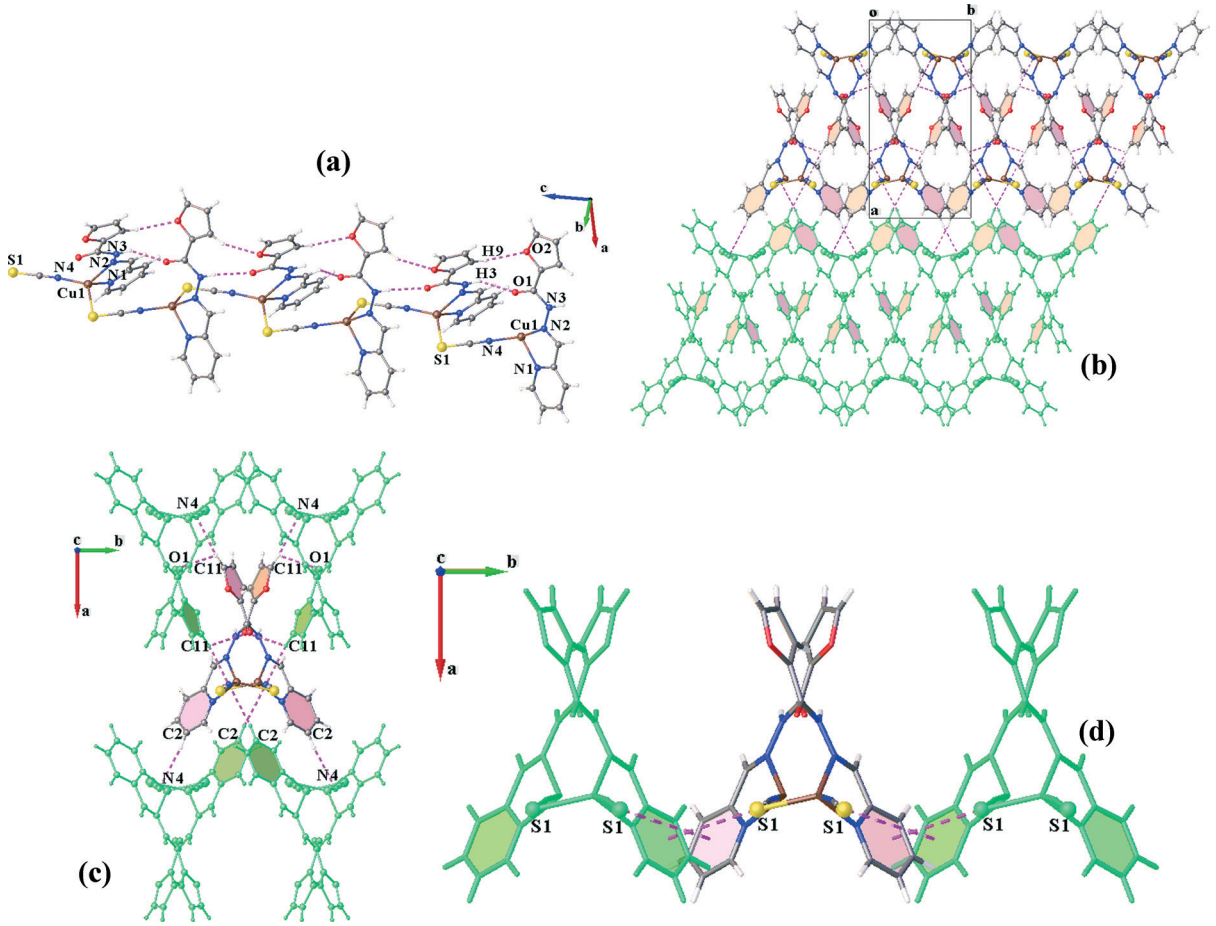

Fig. 6 (a) Intrachain interactions within the coordination polymeric structure of C_{2P} and the side view of the [001] chains to show (b) an overall supramolecular array containing two-fold layers connected to each other; (c) π–π stacking and H-bonding interactions linking a chain to four others and (d) S···π_{py} interactions which connect the chains laterally.

(iv) It was thought to be of interest to further investigate the sulfur interactions to figure out their nature in the solid state structures. The sulfur atom, due to its large van der Waals radius and high polarizability, is able to establish several interactions with its local environment.[46] Morgan and co-workers first proposed the hypothesis that a strong interaction exists between aromatic rings and divalent sulfur atoms.[47] The importance of the S···π aromatic interaction is revealed in the high degree of its conservation across members in protein folding and stabilization.[34,48]

Fig. 8 represents the 3D plots of S···S and S···π interactions in the solid state structures. The compact and small, flat, pill-shaped isosurfaces, concentrated on the NCI critical points indicate that these interactions are significantly attractive and contribute to the crystal packing stability.[45]

Conclusions

Diverse coordination structures from the reaction of CuSCN with PPh_3 and *ortho*-pyridinyl carbohydrazone containing a thiophene (L_1) or furyl ring (L_2) were presented. A mixture of thiocyanate linkage isomers, C_{1N} and C_{1S}, was obtained for L_1, while the reaction with L_2 rendered two monomeric and polymeric compounds, C_{2N} and C_{2P}, respectively. The molecular and supramolecular structures of these systems were elucidated using X-ray diffraction. The structure-directing interactions were also investigated by NCI-RDG calculations.

Pyridine, thiophene and furyl rings, the polarized aromatic systems, have an important role in governing the supramolecular assembly of the complexes by establishing π–π interactions. However, the coordination of sulfur to the Cu(I) atom in C_{1S} leads to supernumerary slippage of the neighbouring molecules which prevents the formation of π_{py}–$\pi_{thiophene}$ connections. CH–π interactions between PPh_3 moieties contribute to further stabilization of the self-association in the monomeric complexes (C_{1N}, C_{1S} and C_{2N}).

A prominent feature of the crystal packing in the monomeric complexes is the formation of the dimeric motifs *via* hydrogen bonding and π–π stacking interactions. Formation of the less stable S-bound isomer C_{1S} can be attributed to stronger intermolecular attractions particularly those involved in dimerization which compensate for the lesser stability of the discrete units of C_{1S} compared to C_{1N}.

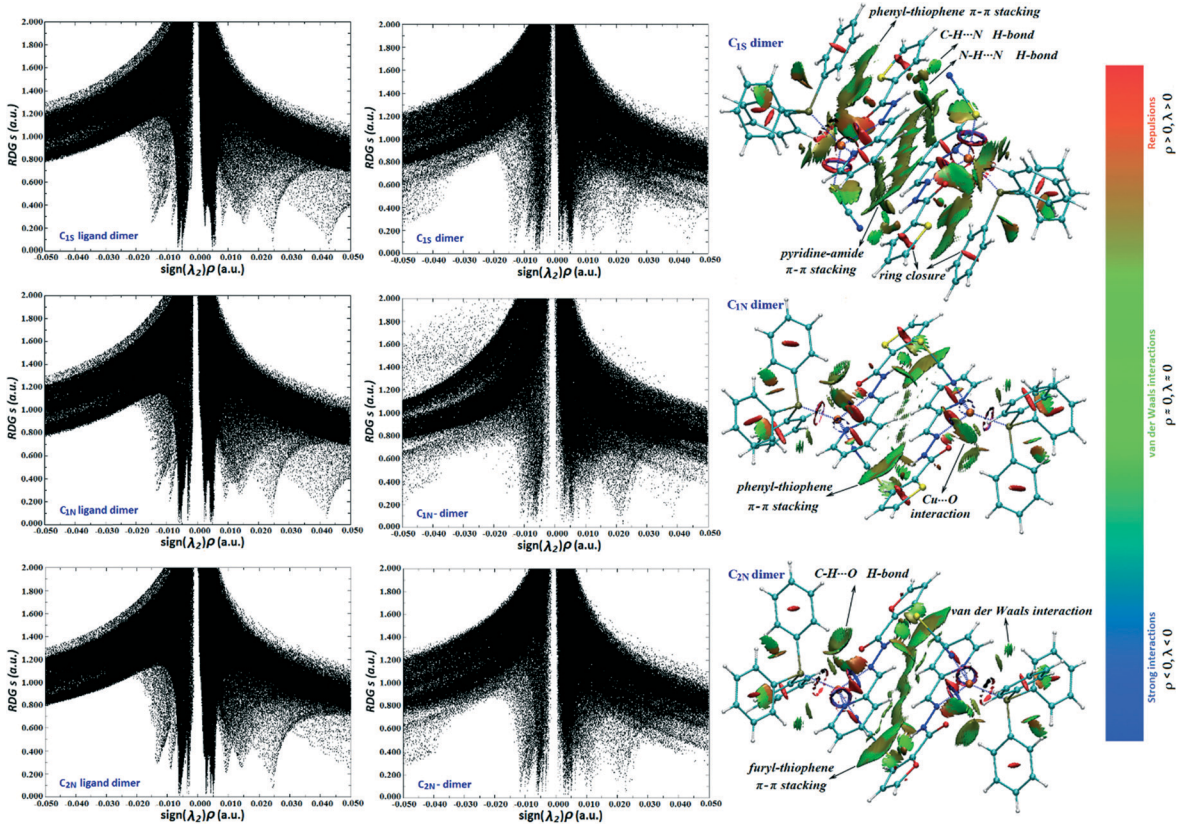

Fig. 7 Left: The NCI RDG *s vs.* sign(λ_2)ρ plots for dimers of ligands and complexes. Right: Coloured RDG-based NCI isosurfaces for the dimers of complexes.

Another interesting feature of the solid state structures is the presence of the lesser known S···S and S···π interactions. NCI-RDG analysis clearly indicates the significant contribution of these interactions in maintaining favourable packing interactions in the complex.

Experimental

Materials and methods

All chemicals and solvents used in the syntheses were of reagent grade and were used without further purification. ^{1}H and ^{13}C NMR spectra were recorded on a Bruker (Avance DRS) 250 MHz spectrometer. IR spectra were recorded on a Nicolet 510P spectrophotometer using KBr disks. Elemental analysis was performed using a Heraeus CHN-O-RAPID apparatus.

Synthesis procedures

The ligands were prepared from the reaction of two equivalent amounts of 2-thiophenecarboxylic acid hydrazide or 2-furoic hydrazide and 2-pyridinecarboxaldehyde in methanol solution.

A solution of ligand (0.20 mmol) in $CHCl_3$ (4 mL) was added dropwise to a stirred solution of a mixture of copper(I) thiocyanate (0.20 mmol) and triphenylphosphine (0.20 mmol) in CH_3CN (2 ml). The colour of the reaction mixture turned from orange to red. The reaction mixture was filtered; slow diffusion of diethyl ether in the filtered solution afforded suitable single crystals (total yields for the mixture of $\mathbf{C_{1N}}$ and $\mathbf{C_{1S}}$: 81%, and for that of $\mathbf{C_{2N}}$ and $\mathbf{C_{2P}}$: 76%). The complexes were obtained in good yields. Physical and spectroscopic data of the compounds are presented below:

(*ortho*-Thiophene)C(O)NHNCH(*ortho*-pyridine) ($\mathbf{L_1}$). Mp: 177–179 °C. Selected IR peaks (cm^{-1}): 3433 w, 3065 w, 1641 s, 1584 m, 1374 s, 1157 m, 733 m. ^{1}H NMR ($CDCl_3$, δ ppm): 7.20–7.35 (m, 2H), 7.73–7.81 (m, 2H), 8.18–8.26 (m, 3H), 8.66 (s, 1H), 10.52 (s, 1H).

(*ortho*-Furyl)C(O)NHNCH(*ortho*-pyridine) ($\mathbf{L_2}$). Mp: 157–160 °C. Selected IR peaks (cm^{-1}): 3422 w, 3005 w, 1662 s, 1579 s, 1468 m, 1308 m, 1187 m, 756 m. ^{1}H NMR ($CDCl_3$, δ ppm): 6.49 (s, 1H), 7.25–7.53 (m, 3H), 7.69 (s, 1H), 8.10 (d, 1H), 8.41–8.55 (d, 2H), 10.64 (s, 1H). ^{13}C NMR ($CDCl_3$, δ ppm): 112.23, 116.32, 121.16, 124.26, 125.69, 136.48, 137.68, 144.82, 148.07, 148.27, 152.81.

[Cu(NCS)($\mathbf{L_1}$)PPh$_3$] ($\mathbf{C_{1N}}$). Orange crystals. Mp: 211–214 °C. Anal. calcd for $C_{30}H_{24}CuN_4OPS_2$: C, 58.57; H, 3.93; N, 9.11. Found: 58.49; H, 3.96; N, 9.17. Selected IR peaks (cm^{-1}): 3437 s, 2925 s, 2003 s, 1670 m, 1540 m, 1431 w, 1264 s, 1142 w, 696 m, 517 w.

[Cu(SCN)($\mathbf{L_1}$)PPh$_3$] ($\mathbf{C_{1S}}$). Red crystals. Mp: 211–213 °C. Anal. calcd for $C_{30}H_{24}CuN_4OPS_2$: C, 58.57; H, 3.93; N, 9.11. Found: 58.41; H, 3.90; N, 9.15. Selected IR peaks (cm^{-1}): 3437 s, 2927 w, 2074 m, 1665 m, 1545 m, 1426 w, 1226 m, 1126 w, 703 m, 512 m.

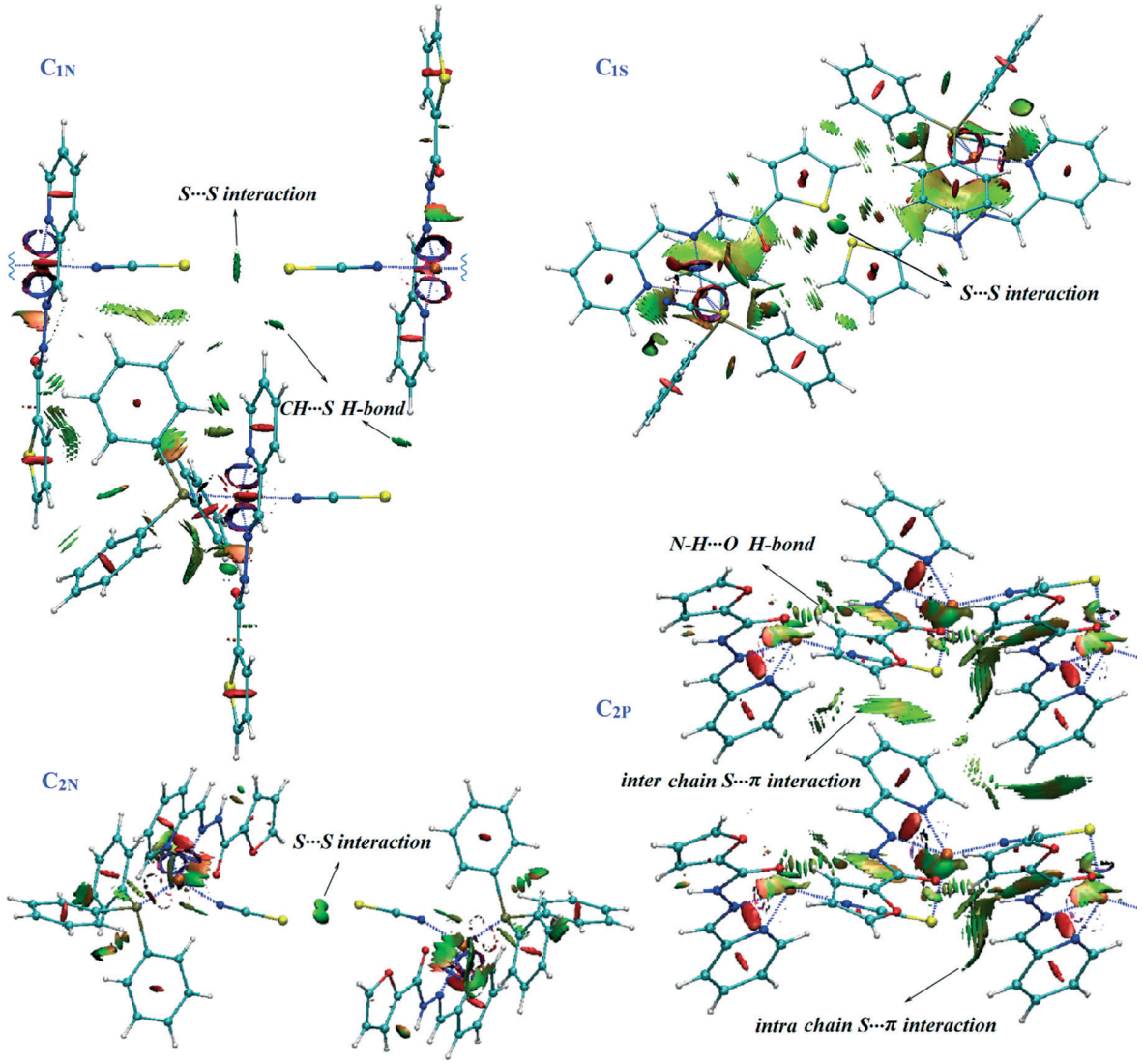

Fig. 8 RDG-based NCI surfaces for S···S and S···π interactions.

[Cu(NCS)(L_2)PPh_3] (C_{2N}). Orange crystals. Mp: 204–206 °C. Anal. calcd for $C_{30}H_{24}CuN_4O_2PS$: C, 60.14; H, 4.04; N, 9.35. Found: 60.21; H, 4.05; N, 9.41. Selected IR peaks (cm^{-1}): 3435 w, 2083 s, 1686 s, 1533 m, 1469 s, 1284 s, 1179 s, 752 m, 696 m, 516 m.

[–(NCS)Cu(L_2)–]$_n$ (C_{2P}). Dark orange crystals. Mp: 238–240 °C (decomp.). Anal. calcd for $C_{12}H_9CuN_4O_2S$: C, 42.79; H, 2.69; N, 16.63. Found: 42.68; H, 2.69; N, 16.60. Selected IR peaks (cm^{-1}): 3277 w, 2112 s, 1672 s, 1543 m, 1464 m, 1295 m, 1186 m, 771 w.

Crystal structure determination

Single crystal X-ray diffraction data were collected for all compounds on an Agilent Gemini Ultra diffractometer equipped with an Eos CCD area detector and using either Mo-Kα radiation (λ = 0.71073 Å) or Cu-Kα radiation (λ = 1.5418 Å). The data were collected at 173 K using an Oxford Cryosystems Cryostream 600. The data were processed with CrysAlisPro.[49] Semi-empirical absorption corrections were carried out using the Multi-Scan[50] program. The structures were solved by direct methods using SHELXT[51] and refined with full matrix least squares refinement using SHELXL-2013 (ref. 52) within Olex2.[53] All non-hydrogen atoms were refined anisotropically. Hydrogen atoms were added at calculated positions and refined using a riding model based on the parent atom. The CIF files have been deposited with the CCDC and have been given the deposition numbers 1401344, 1401345, 1469718 and 1469717 for C_{1N}, C_{1S}, C_{2N} and C_{2p}, respectively.

Computational details

The NCI technique was carried out through the analysis of the reduced density gradient (RDG) with low densities[32] at the ωB97XD[54]/6-311+G** level using the Gaussian 09 package[55] and Multiwfn program.[56] The calculated grid points are plotted for a defined real space function, sign($\lambda_2(r)$)$\rho(r)$ and reduced density gradient (RDG) and a visualization of the

gradient isosurface was depicted using the VMD 1.9.2 software.[57] The colour of the isosurfaces was decided using the value of sign(λ_2)ρ. Blue, green and red colour codes are commonly used to describe stabilizing H-bonding, van der Waals and steric interaction, respectively. Pictures are provided for an isosurface value of s = 0.5.

Natural bond orbital (NBO) analysis[58] was performed on the crystal structure of the complexes using the NBO 3.1 module in Gaussian 09 at the B3LYP/6-311+G** level of theory. The binding energy of two complexes in a dimer, ΔE_{dimer}, for C_{1N}, C_{1S} and C_{2N} were calculated at the M062X/6-311G* level based on the energy difference between the dimer and its units. The interaction energies have been corrected for the basis set superposition error (BSSE) using the counterpoise (CP) procedure.[59]

Acknowledgements

Financial support of this work by Tarbiat Modares University is gratefully acknowledged.

Notes and references

1 N. Aoyagi, Y. Shinha, A. Ikeda-Ohno, Y. Haga, K. Shimojo, N. R. Brooks, A. Izuoka, H. Naganawa, T. Kimura and K. Binnemans, *Cryst. Growth Des.*, 2015, **15**, 1422.
2 E. T. Spielberg, E. Edengeiser, B. Mallick, M. Havenith and A.-V. Mudring, *Chem. – Eur. J.*, 2014, **20**, 5338.
3 C. S. Smith, C. W. Branham, B. J. Marquardt and K. R. Mann, *J. Am. Chem. Soc.*, 2010, **132**, 14079.
4 L. Li, P. S. Lopes, V. Rosa, C. A. Figueira, M. A. N. D. A. Lemos, M. T. Duarte, T. Avilés and P. T. Gomes, *Dalton Trans.*, 2012, **41**, 5144.
5 P. J. Pérez and M. M. Díaz-Requejo, in *Comprehensive Organometallic Chemistry III*, ed. R. H. Crabtree and D. M. P. Mingos, Elsevier, New York, 2007, vol. 2, pp. 153–195.
6 S. E. Allen, R. R. Walvoord, R. Padilla-Salinas and M. C. Kozlowski, *Chem. Rev.*, 2013, **113**, 6234.
7 A. Ouali, J.-F. Spindler, H.-J. Cristau and M. Taillefer, *Adv. Synth. Catal.*, 2006, **348**, 499.
8 D. G. Cuttell, S.-M. Kuang, P. E. Fanwick, D. R. McMillin and R. A. Walton, *J. Am. Chem. Soc.*, 2002, **124**, 6.
9 T. McCormick, W.-L. Jia and S. Wang, *Inorg. Chem.*, 2006, **45**, 147.
10 R. Czerwieniec and H. Yersin, *Inorg. Chem.*, 2015, **54**, 4322.
11 L. Kang, J. Chen, T. Teng, X.-L. Chen, R. Yu and C.-Z. Lu, *Dalton Trans.*, 2015, **44**, 11649.
12 D. Volz, M. Nieger, J. Friedrichs, T. Baumann and S. Bräse, *Langmuir*, 2013, **29**, 3034.
13 G. F. Manbeck, W. W. Brennessel, C. M. Evans and R. Eisenberg, *Inorg. Chem.*, 2010, **49**, 2834.
14 J. C. Deaton, S. C. Switalski, D. Y. Kondakov, R. H. Young, T. D. Pawlik, D. J. Giesen, S. B. Harkins, A. J. M. Miller, S. F. Mickenberg and J. C. Peters, *J. Am. Chem. Soc.*, 2010, **132**, 9499.
15 Z. Liu, P. I. Djurovich, M. T. Whited and M. E. Thompson, *Inorg. Chem.*, 2012, **51**, 230.
16 M. J. Leitl, F.-R. Küchle, H. A. Mayer, L. Wesemann and H. Yersin, *J. Phys. Chem. A*, 2013, **117**, 11823.
17 D. M. Zink, T. Baumann, J. Friedrichs, M. Nieger and S. Bräse, *Inorg. Chem.*, 2013, **52**, 13509.
18 D. Volz, T. Baumann, H. Flügge, M. Mydlak, T. Grab, M. Bächle, C. Barner-Kowollik and S. Bräse, *J. Mater. Chem.*, 2012, **22**, 20786.
19 D. Volz, M. Wallesch, S. L. Grage, J. Göttlicher, R. Steininger, D. Batchelor, T. Vitova, A. S. Ulrich, C. Heske, L. Weinhardt, T. Baumann and S. Bräse, *Inorg. Chem.*, 2014, **53**, 7837.
20 L. Bergmann, J. Friedrichs, M. Mydlak, T. Baumann, M. Nieger and S. Bräse, *Chem. Commun.*, 2013, **49**, 6501.
21 X. Liu, H. Nan, W. Sun, Q. Zhang, M. Zhan, L. Zou, Z. Xie, X. Li, C. Lu and Y. Cheng, *Dalton Trans.*, 2012, **41**, 10199.
22 D. Volz, D. M. Zink, T. Bocksrocker, J. Friedrichs, M. Nieger, T. Baumann, U. Lemmer and S. Bräse, *Chem. Mater.*, 2013, **25**, 3414.
23 A. Hazari, L. Kanta Das, A. Bauzá, A. Frontera and A. Ghosh, *Dalton Trans.*, 2014, **43**, 8007.
24 R. Loos, S. Kobayashi and H. Mayr, *J. Am. Chem. Soc.*, 2003, **125**, 14126.
25 L. Vandenburgh, M. R. Buck and D. A. Freedman, *Inorg. Chem.*, 2008, **47**, 9134.
26 M. J. Maroney, E. O. Fey, D. A. Baldwin, R. E. Stenkamp, L. H. Jensen and N. J. Rose, *Inorg. Chem.*, 1986, **25**, 1409.
27 A. D. Martin, J. Britton, T. L. Easun, A. J. Blake, W. Lewis and M. Schröder, *Cryst. Growth Des.*, 2015, **15**, 1697.
28 K. Gholivand, K. Farshadfar, S. M. Roe, A. Gholami and M. D. Esrafili, *CrystEngComm*, 2016, **18**, 2873.
29 P. Qin, S. Tanaka, S. Ito, N. Tetreault, K. Manabe, H. Nishino, M. K. Nazeeruddin and M. Grätzel, *Nat. Commun.*, 2014, 1.
30 T. P. Brewster, W. Ding, N. D. Schley, N. Hazari, V. S. Batista and R. H. Crabtree, *Inorg. Chem.*, 2011, **50**, 11938.
31 K. M. Miller, S. M. McCullough, E. A. Lepekhina, I. J. Thibau, R. D. Pike, X. Li, J. P. Killarney and H. H. Patterson, *Inorg. Chem.*, 2011, **50**, 7239.
32 E. R. Johnson, S. Keinan, P. Mori-Sanchez, J. Contreras-Garcia, A. J. Cohen and W. Yang, *J. Am. Chem. Soc.*, 2010, **132**, 6498.
33 (*a*) L. Wang, Y. Hu, W. Wang, F. Liu and K. Huang, *CrystEngComm*, 2014, **16**, 4142; (*b*) K. I. Nättinen and K. Rissanen, *Cryst. Growth Des.*, 2003, **3**, 339; (*c*) B. Piotrkowska, A. Wasilewska, M. Gdaniec and T. Polonski, *CrystEngComm*, 2008, **10**, 1421; (*d*) E. Bosch, N. P. Bowling and J. Darko, *Cryst. Growth Des.*, 2015, **15**, 1634; (*e*) C. B. Aakeröy, D. J. Salmon, M. M. Smith and J. Desper, *Cryst. Growth Des.*, 2006, **6**, 1033; (*f*) A. Lemmerer, D. A. Adsmond, C. Esterhuysen and J. Bernstein, *Cryst. Growth Des.*, 2013, **13**, 3935.
34 B. R. Beno, K.-S. Yeung, M. D. Bartberger, L. D. Pennington and N. A. Meanwell, *J. Med. Chem.*, 2015, **58**, 4383.
35 (*a*) H. Akpinar, J. T. Mague and P. M. Lahti, *CrystEngComm*, 2013, **15**, 831; (*b*) M. M. Naseer and S. Hameed, *CrystEngComm*, 2012, **14**, 4247; (*c*) B. Sarma, L. S. Reddy and

A. Nangia, *Cryst. Growth Des.*, 2008, **8**, 4546; (*d*) C. Janiak, *J. Chem. Soc., Dalton Trans.*, 2000, 3885.

36 (*a*) M. Nishio, Y. Umezawa, K. Honda, S. Tsuboyama and H. Suezawa, *CrystEngComm*, 2009, **11**, 1757; (*b*) M. Nishio, M. Hirota and Y. Umezawa, *The CH/π Interaction. Evidence, Nature, and Consequences*, Wiley-VCH, New York, 1998; (*c*) M. Nishio, *CrystEngComm*, 2004, **6**, 130; (*d*) M. Umezawa, S. Tsuboyama, K. Honda, J. Uzawa and M. Nishio, *Bull. Chem. Soc. Jpn.*, 1998, **71**, 1207.

37 L. Yang, D. R. Powell and R. P. Houser, *Dalton Trans.*, 2007, 955.

38 S. Pan, S. Mandal and P. K. Chattaraj, *J. Phys. Chem. B*, 2015, **119**, 10962.

39 P. R. Varadwaj, A. Varadwaj and B.-Y. Jin, *Phys. Chem. Chem. Phys.*, 2014, **16**, 17238.

40 P. R. Varadwaj, A. Varadwaj and B.-Y. Jin, *Phys. Chem. Chem. Phys.*, 2014, **16**, 19573.

41 K. Saadat and H. Tavakol, *RSC Adv.*, 2015, **5**, 55227.

42 R. P. Matthews, T. Welton and P. A. Hunt, *Phys. Chem. Chem. Phys.*, 2015, **17**, 14437.

43 Y. Chu, X. Sun, Y. Xianfeng, L. Ding, A. Zheng and F. Deng, *Catal. Sci. Technol.*, 2015, **5**, 3507.

44 P. R. Varadwaj, A. Varadwaj and B.-Y. Jin, *Phys. Chem. Chem. Phys.*, 2015, **17**, 31624.

45 R. Chaudret, B. de Courcy, J. Contreras-Garcia, E. Gloaguen, A. Zehnacker-Rentien, M. Mons and J.-P. Piquemal, *Phys. Chem. Chem. Phys.*, 2014, **16**, 9876.

46 G. Saleh, C. Gatti, L. L. Presti and J. Contreras-Garcia, *Chem. – Eur. J.*, 2012, **18**, 15523.

47 R. S. Morgan, C. E. Tatsch, R. H. Gushard, J. M. McAdon and P. K. Warme, *Int. J. Pept. Protein Res.*, 1978, **11**, 209.

48 R. Bhattacharyya, D. Pal and P. Chakrabarti, *Protein Eng., Des. Sel.*, 2004, **17**, 795.

49 *CrysAlisPro, Agilent Technologies*, Yarnton, England, 2014.

50 R. H. Blessing, *Acta Crystallogr., Sect. A: Found. Crystallogr.*, 1995, **51**, 33.

51 G. M. Sheldrick, *Acta Crystallogr., Sect. A: Found. Adv.*, 2015, **71**, 3.

52 G. M. Sheldrick, *Acta Crystallogr., Sect. C: Struct. Chem.*, 2015, **71**, 3.

53 O. V. Dolomanov, L. J. Bourhis, R. J. Gildea, J. A. K. Howard and H. Puschmann, *J. Appl. Crystallogr.*, 2009, **42**, 339.

54 J. D. Chai and M. H. Gordon, *Phys. Chem. Chem. Phys.*, 2008, **10**, 6615.

55 M. J. Frisch, G. W. Trucks, H. B. Schlegel, G. E. Scuseria, M. A. Robb, J. R. Cheeseman, G. Scalmani, V. Barone, B. Mennucci, G. A. Petersson, H. Nakatsuji, M. Cari-cato, X. Li, H. P. Hratchian, A. F. Izmaylov, J. Bloino, G. Zheng, J. L. Sonnenberg, M. Hada, M. Ehara, K. Toyota, R. Fukuda, J. Hasegawa, M. Ishida, T. Nakajima, Y. Honda, O. Kitao, H. Nakai, T. Vreven, J. A. Montgomery Jr., J. E. Peralta, F. Ogliaro, M. Bearpark, J. J. Heyd, E. Brothers, K. N. Kudin, V. N. Staroverov, R. Kobayashi, J. Normand, K. Raghavachari, A. Rendell, J. C. Burant, S. S. Iyengar, J. Tomasi, M. Cossi, N. Rega, J. M. Millam, M. Klene, J. E. Knox, J. B. Cross, V. Bakken, C. Adamo, J. Jaramillo, R. Gomperts, R. E. Stratmann, O. Yazyev, A. J. Austin, R. Cammi, C. Pomelli, J. W. Ochterski, R. L. Martin, K. Morokuma, V. G. Zakrzewski, G. A. Voth, P. Salvador, J. J. Dannenberg, S. Dapprich, A. D. Daniels, Ö. Farkas, J. B. Foresman, J. V. Ortiz, J. Cioslowski and D. J. Fox, *Gaussian 09, Revision D.01*, Gaussian, Inc., Wallingford, CT, 2009.

56 T. Lu and F. J. Chen, *Comput. Chem.*, 2012, **33**, 580.

57 W. Humphrey, A. Dalke and K. Schulten, *J. Mol. Graphics*, 1996, **14**, 33.

58 A. E. Reed, L. A. Curtiss and F. Weinhold, *Chem. Rev.*, 1988, **88**, 899.

59 S. F. Boys and F. Bernardi, *Mol. Phys.*, 1970, **19**, 553.